ACS SENSORS

pubs.acs.org/acssensors

Article

Open Access

This article is licensed under CC-BY 4.0

Tethered Split-Aptamer Biosensor for Plasmon-Enhanced Fluorescence-Based Continuous Monitoring of Vancomycin

Gizem Aktug, Naoto Asai, Anil Bozdogan, Catia Santa, Khulan Sergelen, and Jakub Dostalek*

Cite This: *ACS Sens.* 2026, 11, 1348−1357

Read Online

ACCESS | Metrics & More | Article Recommendations | Supporting Information

ABSTRACT: A split aptamer assay with plasmon-enhanced fluorescence readout is reported for continuous monitoring of low-molecular-weight analytes. The sensor was implemented by using a biointerface with the first split aptamer segment (S1) anchored to the metal sensor surface via a DNA-based flexible polymer linker (FPL) and the second split aptamer segment (S2) directly attached to this surface. The affinity interaction of S1 and S2 with the target analyte modulates the distance between the metallic surface and a fluorophore attached to the FPL outer end. This translates to detected variations in fluorescence signal intensity due to the competing quenching and plasmonic enhancement of emitted fluorescence light. By controlling the surface concentrations of split aptamer segments, the affinity interaction between S1, S2, and the target analyte can be tuned, and key assay characteristics can be modulated over a wide range. For the target antibiotic vancomycin, the respective effective equilibrium dissociation constant was varied by two orders of magnitude from nM to μM concentrations. Despite a fast dissociation rate being necessary for continuous monitoring of the target analyte, the limit of detection could be tuned to low nM concentrations, constituting a concept that can be straightforwardly adapted for other assays that take advantage of reversible affinity interactions with surface-confined split aptamers.

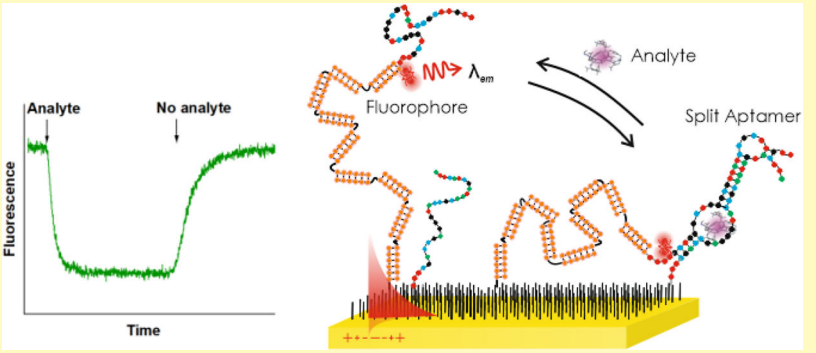

KEYWORDS: *split aptamer, flexible polymer linker, surface-plasmon-enhanced fluorescence, continuous monitoring, biosensor, vancomycin*

Downloaded via INST PHYSICS CZECH ACADEMY SCIENCES on March 2, 2026 at 07:59:40 (UTC).
See https://pubs.acs.org/sharingguidelines for options on how to legitimately share published articles.

Continuous monitoring of chemical compounds has gained increasing attention in recent years owing to its potential to advance biomedical diagnostics, personalized therapy, and environmental analysis. Current research has addressed these needs through the development of various sensing concepts, including optical tracking of microparticles capable of reversibly and quantitatively detecting short single-stranded oligos and creatinine;[1] an electrochemical sensor with an active-reset sensor mechanism, enabling rapid, continuous in vivo monitoring of protein biomarkers;[2] and a FRET-based DNA-scaffolded antibody switch, serving in competitive optical biosensors for small molecules, such as cortisol and digoxigenin.[3] In addition to these advances, plasmon-enhanced fluorescence (PEF)-based readout with a sandwich assay format demonstrated single-molecule sensitivity and reversible tracking of analytes, including cancer-related DNA markers, directly in biological fluids.[4]

Such progress is paving the way toward continuous molecular monitoring platforms that hold the potential to revolutionize therapeutic drug monitoring (TDM). By providing real-time drug concentration readouts for immediate dose adjustment, biosensors can offer a path to precision pharmacotherapy that minimizes toxicity, prevents drug resistance, and improves patient outcomes across diverse classes of therapeutics, including antibiotics, antivirals, and anti-inflammatory and anticancer agents.[5,6] Electrochemical sensors have emerged as useful tools for pharmacokinetic profiling,[7,8,9] and they mostly implement continuous monitoring of therapeutic drugs by using two main mechanisms to generate an electrochemical signal: enzymatic catalysis or aptamer affinity recognition. Aptamer-based sensors exploit the specific binding of target molecules by short DNA and RNA oligo sequences, and in electrochemical biosensors, they are typically conjugated with a redox reporter.[8] Based on a conformational change upon analyte binding, the proximity or orientation of the conjugated redox reporter relative to the electrode surface leads to a change in measured electron transfer efficiency. By using such an approach, real-time monitoring of doxorubicin (a chemotherapeutic) and aminoglycoside-based detection

Received: September 29, 2025
Revised: December 18, 2025
Accepted: January 5, 2026
Published: February 6, 2026

ACS Publications

© 2026 The Authors. Published by American Chemical Society

https://doi.org/10.1021/acssensors.5c03606
ACS Sens. 2026, 11, 1348−1357

of kanamycin, gentamicin, and tobramycin (antibiotics) were performed at clinically relevant concentrations.[10]

In recent years, researchers have increasingly focused on monitoring another antibiotic, vancomycin, by exploiting aptamers.[9,11,12,13] Vancomycin is a clinically important antibiotic (with a molecular weight of 1449 Da), which is widely used in the treatment of severe infections caused by Gram-positive bacteria,[14] and has a narrow therapeutic window.[15,16] Through parent aptamer truncations, Dauphin-Ducharme et al. produced an optimal DNA aptamer that binds to vancomycin and undergoes a conformational change, which allows an electrochemical detection with an equilibrium dissociation constant (K_d) of 45 μM in a whole blood sample.[9] Building on this, a series of aptamer truncations was tested to improve the sensitivity and dynamic range of the sensor.[11] Consequently, extending the truncated aptamer by one base pair improved the affinity with a K_d of 11.7 μM and enhanced the sensor performance. In addition to such truncation strategies, researchers have also employed split aptamers, comprising two or more fragments derived from the parent sequence, in optical continuous biosensing. Unlike the structure-switching full-length parent aptamers, split aptamers are shorter, facilitating easier synthesis and potentially offering the advantage of improved specificity and sensitivity for the target analyte.[17] By using this approach, a sandwich assay enabling real-time, reversible, and label-free optical detection of vancomycin using surface plasmon resonance (SPR) was introduced.[12] By identifying an optimal split site and varying split segment interaction, the target affinity was significantly enhanced, achieving a K_d of 2.2 μM and an LOD of 140 nM in biological fluids. By employing the identical split aptamers, a direct, stable, and reversible biosensing platform with split-aptamer-functionalized hydrogels, aptagels, was developed for continuous in vivo detection of vancomycin with an LOD of 160−250 nM and a wide detection range up to 1 mM.[13]

In this report, we investigate a biointerface architecture with a DNA-based flexible polymer linker (FPL) for the split aptamer assay that is designed for direct continuous monitoring of low-molecular-weight analytes, such as vancomycin. The surface PEF method was used in a configuration that allows controlling the surface concentration ratio of split aptamers and relies on their immobilization at different distances from the sensor surface. Key parameters in the assay are investigated with a well-characterized aptamer sequence specific to the low-molecular-weight antibiotic vancomycin in a split version.[12,13] By design of the interface and with a two-step biomolecular interaction model, we elucidate that the effective equilibrium dissociation constant for the specific interaction with the target analyte is tunable over several orders of magnitude, which allows for shifting the detection range and LOD. For optimized conditions, the LOD can be improved by more than an order of magnitude when compared to other works that implemented the same split aptamer pair with optical and electrochemical readout methods relying on modulation of the distance between the sensor surface and aptamer ligands.[9,11,12,13] The presented results reveal the utmost importance of the biointerface design for the optimization and tuning of the LOD and detection range. It offers high versatility in the split aptamer assay format and can be adapted to other assays using the theoretical model established herein, which captures the surface-confined affinity interaction between the split aptamer segments and the target analyte.

EXPERIMENTAL SECTION

Biointerface

The sensor surface was functionalized with neutravidin (NA), dissolved at 50 μg/mL (833 nM), via high-affinity binding for 20 min to the thiol self-assembled monolayer (SAM) surface that contains biotin moieties. Optionally, a multilayer of biotinylated bovine serum albumin (B-BSA) and NA was adsorbed onto the NA-coated surface to adjust the distance from the surface d_0 (see Figure 1). Following NA immobilization, 10 nM of the FPL, consisting of the biotin-tagged St_5 (B-St_5) sequence on one end (see Table S1) and Cy5-tagged split aptamer 1 (Cy5-S1) on the other, was attached to the surface by a 2-min reaction with NA. Subsequently, 1 nM biotinylated split aptamer 2 (B-S2) was incubated on the surface for 6 min to backfill remaining available NA binding sites.

Preparation of the FPL

The formation of the DNA-based FPL, composed of nine single-stranded DNA (ssDNA) strands (see Table S1) with a total length

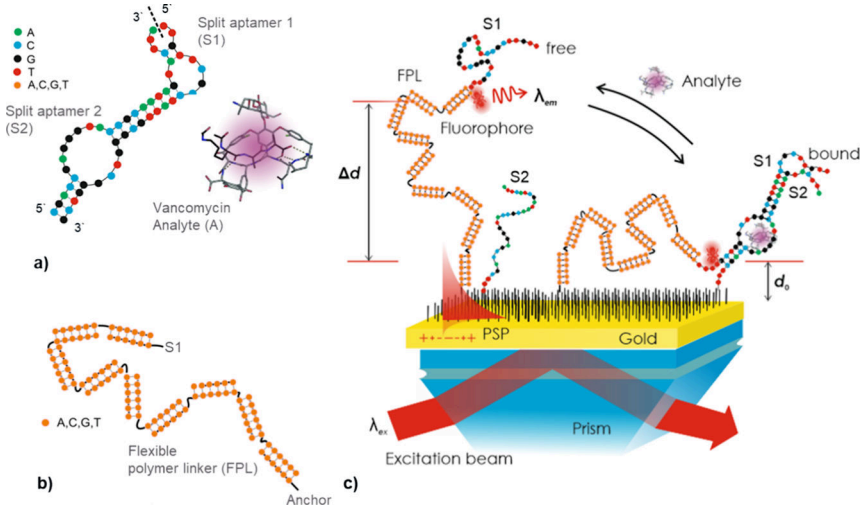

Figure 1. (a) Schematics of the used aptamer sequence specific for vancomycin that was split into two segments, S1 and S2. (b) Design of the FPL composed of rigid dsDNA segments connected by flexible ssDNA hinges. (c) Biointerface where the S1 aptamer segment is anchored via the FPL and S2 is directly attached to the surface for surface PEF readout of affinity interaction-induced changes in distance between a fluorophore conjugated with the FPL at its outer tip and the metallic sensor surface.

https://doi.org/10.1021/acssensors.5c03606
ACS Sens. 2026, 11, 1348−1357

of 445 nucleotides, was adapted from Asai et al.[18] with minor modifications. For the assembly, individual ssDNAs, together with Cy5-S1, were allowed to react in a solution of 10 mM PBS supplemented with 2 mM $MgCl_2$ (working buffer, degassed before use, sequence of oligo additions specified in Table S2). The mixture was subjected to thermal annealing, followed by gradual cooling from an elevated temperature (95 °C) to promote correct hybridization. After annealing, the assembled FPL constructs were stored protected from light at +4 °C until further use.

Optical Readout

A combined SPR and surface PEF spectroscopy system built in the Kretschmann configuration was used to observe the biointerface preparation and split aptamer–analyte interaction. For these measurements, a laser with an excitation wavelength of λ_{ex} = 633 nm was used to excite the Cy5 fluorophore with the enhanced field intensity in PEF readout. The fluorescence emission intensity was then detected at a Stokes-shifted wavelength of λ_{em} = 670 nm in counts per second (cps). In parallel, the fluorescence measurements can be complemented by following changes in the SPR coupling angle in order to capture variations in biomolecule surface mass density from binding-induced changes in refractive index expressed in milli refractive index units (mRIU).

Aptamer Sandwich Assay

After the assembly of the biointerface with FPL-S1 and S2 aptamers, vancomycin analyte solutions at nM–μM concentrations were flowed over the sensor surface. All components, washing steps, and human plasma dilutions were employed in the working buffer. To prove the specific interaction of the chosen aptamer segment, a shuffled variant of S1 was generated by using an online DNA shuffling tool,[19] which conserves the nucleotide composition but rearranges the positions of the nucleotides. Specificity of the assay was confirmed by employing bacitracin as a negative control analyte.

RESULTS AND DISCUSSION

The pursued sensor concept relies on the optical readout of conformational change of an aptamer triggered by its affinity interaction with the target analyte, and as shown in Figure 1a, we used such an aptamer sequence that was split into two segments (as previously reported for vancomycin-binding aptamers,[12,13]). To spatially confine the affinity reaction between the split aptamer segments and the analyte (A) on the gold sensor surface, the first split aptamer segment S1 was anchored on it via an FPL and the second split aptamer segment S2 was attached directly in its close proximity. Based on our previous works, and as seen in Figure 1b, the FPL was prepared from a series of nine rigid double-stranded DNA (dsDNA) elements connected via flexible single-stranded DNA (ssDNA) hinges[18] in order to prolong the distance between the unbound S1 aptamer sequence from the sensor surface. The tip of the FPL that is conjugated with split aptamer S1 was modified by fluorophore Cy5, and its distance-dependent fluorescence emission intensity F was monitored. It allowed us to establish the transducing mechanism that relies on the strong distance-dependent competing effects of fluorescence quenching and fluorescence enhancement[20] induced by reversible association and dissociation of S1–S2 mediated by the specific interaction with target analyte A. The affinity interaction of S1 and S2 aptamer segments with target analyte A affects the stability of the S1–S2 complex and thus can be detected from measured fluorescence intensity variations ΔF. Figure 1c shows a schematic of such a readout by using a biointerface, where S2 was immobilized at a short distance d_0 from the gold sensor surface, while the unbound Cy5-tagged S1 is allowed to diffuse in an average longer distance $d_0 + \Delta d$ defined by the length and flexibility of the FPL. When S1 and S2 form a complex, the emitter at the outer tip of the FPL is forced to stay at a short distance d_0, and the respective residence time is prolonged when the S1–S2 complex binds target analyte A from the analyzed sample brought in contact with the surface. To enhance the detected fluorescence intensity F, the biointerface was probed at the Cy5 fluorophore excitation wavelength λ_{ex} with an optical beam that was resonantly coupled to propagating surface plasmons (PSPs) traveling along the gold sensor interface. The resonant PSP excitation provides enhanced electromagnetic field intensity at the excitation wavelength λ_{ex}, and it was utilized in the Kretschmann configuration of the attenuated total reflection method. The fluorescence light intensity F at the fluorophore emission wavelength, λ_{em}, emitted perpendicular to the sensor surface, was collected and detected in real time.

Assembly of the Biointerface

Combined SPR and PEF measurements were used to monitor the biointerface assembly and to determine the surface density of functional biomolecules. Figure 2a presents typical kinetics of

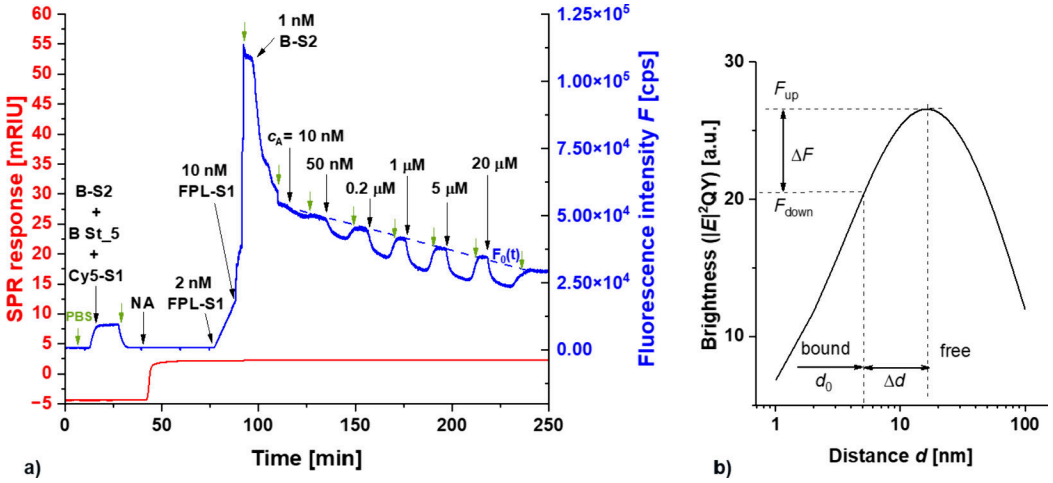

Figure 2. (a) Example of the sensorgram for the assembly of the biointerface carrying FPL-S1 conjugated with a fluorophore and B-S2 at controlled density atop a monolayer of NA. (b) Model describing the emitter brightness as a function of its distance from the gold sensor surface, incorporating both plasmon-enhanced excitation and quenching effects.

https://doi.org/10.1021/acssensors.5c03606
ACS Sens. 2026, 11, 1348–1357

the SPR response plotted in refractive index changes (red curve), together with the fluorescence signal F (blue curve). The gold sensor surface was modified with a thiol SAM-bearing biotin group, together with hydrophilic PEG, forming a low-fouling carpet. In the first control experiment, Cy5-S1 was flowed together with the anchoring part of FPL (B-St_5) and S2 (100 nM each) for 15 min over the thiol-SAM-modified surface to check nonspecific adsorption. The acquired results show no measurable SPR change and only an increased fluorescence signal that can be ascribed to the excitation of fluorophores present in the bulk. After washing with the working buffer, the fluorescence signal returned to the original baseline, indicating no binding of the oligo to the surface. In the second step, NA was bound to the biotin groups for further immobilization of FPL-S1 and S2. The large biotin-tagged FPL-S1 (molecular weight of 2.67×10^2 kDa) was dissolved at concentrations of 2 and 10 nM and in total flowed over the surface for 15 min, and the respective fluorescence signal increased by about 10^5 cps. The SPR signal increased by 1.2×10^{-1} mRIU (see details in Figure S1), and it corresponds to a surface mass density of $\Delta\Gamma = 5.7 \times 10^{-2}$ ng/mm^2 and a surface density of 1.2×10^2 copies/μm^2 (details on translating the SPR change to these quantities can be found in the Supporting Information, Section 2). Afterward, the surface was reacted for 5 min with 1 nM biotin-tagged S2 oligo (B-S2, molecular weight of 14.4 kDa), and the obtained sensorgram revealed a slight increase in the SPR signal of 1.7×10^{-2} mRIU (see details in Figure S1) corresponding to its surface density of 4×10^2 copies/μm^2.

Upon the immobilization of B-S2, a decrease in fluorescence intensity F by about 30% occurs. It can be attributed to the hybridization of S1 and S2, which brings the emitter from a further distance $d_0 + \Delta d$ to a closer proximity to the gold surface d_0. Figure 2b shows a model that simulates the brightness of an emitter depending on the distance. It takes into account the spatial dependence of the excitation evanescent surface plasmon field intensity $|E|^2$ at λ_{ex} and the effect of Förster energy transfer quenching, decreasing the emitter quantum yield at λ_{em} (data for a randomly oriented emitter taken from our previous publications[20,21]). This model predicts that when changing the distance from $d_0 \sim 5$ nm (estimated from the size of the NA and the thickness of the thiol SAM) to $d_0 + \Delta d \sim 20$ nm (where the maximum brightness occurs), the maximum fluorescence intensity changes by about 23%. This value is comparable to the measured fluorescence intensity variations and differs due to phenomena not captured by the model (such as roughness of the surface and deviations in the distances depending on not accurately known molecular orientations and flexibility of the involved linkers).

Afterward, the sensor surface was reacted with a series of working buffer samples spiked with target analyte A concentrations of 10 nM–20 μM, with washing steps in between. The obtained sensorgram showing measured fluorescence intensity changes in Figure 2a indicates that the analyte binding to the S1–S2 duplex causes a further decrease in fluorescence intensity, attributed to the fluorophore being locked for a prolonged time in close proximity to the metal surface, distance d_0. In addition, Figure 2a shows that the affinity interaction with the target analyte is reversible, as upon the washing step, the response returns to the baseline F_0. Moreover, it is apparent that the fluorescence signal baseline F_0 gradually decreases in time due to the effect of photo bleaching (fitted with an exponential function). Even though this effect reduces the overall lifetime of the sensor, it was possible to operate it for >9 h, and let us note that this drawback can be substantially improved by using another emitter than Cy5 (which was chosen for the availability of internal labeling of oligos), such as AlexaFluor 647, which exhibits better photostability.[22]

REVERSIBLE SPLIT APTAMER ASSAY

In further analysis, we describe the affinity interaction between S1, S2, and target analyte A, as illustrated in Figure 3a. We assume that there is negligible direct interaction between individual S1 or S2 and analyte A. In addition, we set that S1 binds to S2 with an equilibrium association constant K_d^A, as their structures bear two segments with nine- and five-nucleotide-long complementary sequences. The hybridized S1–S2 complex forms the functional aptamer that binds the target analyte A with another equilibrium association constant K_d^B.

Direct interaction between S1 and S2 is confirmed in the experiment, where B-S2 was directly immobilized on the gold sensor surface via a biotin tag, and the S1 aptamer segment was conjugated with a fluorophore tag and reacted with the surface when dissolved in the working buffer at a concentration of $c_{S1} =$ 100 nM. As shown in Figure 3b, the fluorescence signal gradually increases and approaches saturation after 15 min of reaction. When the surface is rinsed with a working buffer, the fluorescence intensity F gradually decreases to the original baseline due to the dissociation of the S1–S2 complex. A control experiment with a shuffled S1 sequence tagged with the same fluorophore at a concentration of 100 nM shows only a rapid increase and decrease in the fluorescence intensity due to the excitation of fluorescence in the bulk solution.

In a further step, the same biointerface with an anchored S2 aptamer segment at a distance d_0 was reacted with a working buffer containing target analyte A present at a concentration varying from $c_A = 50$ nM to 100 μM and S1 at a fixed concentration of $c_{S1} = 100$ nM. The obtained kinetics of the fluorescence signal are presented in Figure 3c, and they reveal that the presence of the target analyte leads to an increased fluorescence signal F due to the higher amount of the S1 aptamer segment bound to the sensor surface. Importantly, the rinsing step with a working buffer after a 40 min incubation leads to the release of the S1 aptamer from the surface, accompanied by a decrease in the fluorescence signal to the original baseline within 20 min. Let us note that the observed trends qualitatively agree with a previous SPR study (carried out with a higher $c_{S1} = 2$ μM)[12] and the kinetics measured here are strongly limited by diffusion-driven mass transfer.

Afterward, we carried out the experiment with a biointerface that carries both aptamer segments confined on the surface. In this architecture, the S2 segment was immobilized directly at the distance d_0, and S1 was anchored at an elevated distance $d_0 + \Delta d$ via FPL. Both aptamer segments S1 and S2 were allowed to react with the target analyte dissolved in a working buffer at concentrations increasing from $c_A = 5$ nM to 5 μM. As can be seen in Figure 3d, the sensor responds to the presence of analyte A faster (within several minutes) compared to the previous bulk configuration (equilibrium not reached in 40 min), and its binding at the sensor surface is manifested as a decrease in the fluorescence signal (presented as normalized to a baseline F/F_0). Similar to the configuration with S1 present in the bulk solution, the interaction with the target analyte is fully reversible, and the complex S1-S2-A dissociates within several minutes when rinsing with the working buffer.

https://doi.org/10.1021/acssensors.5c03606
ACS Sens. 2026, 11, 1348−1357

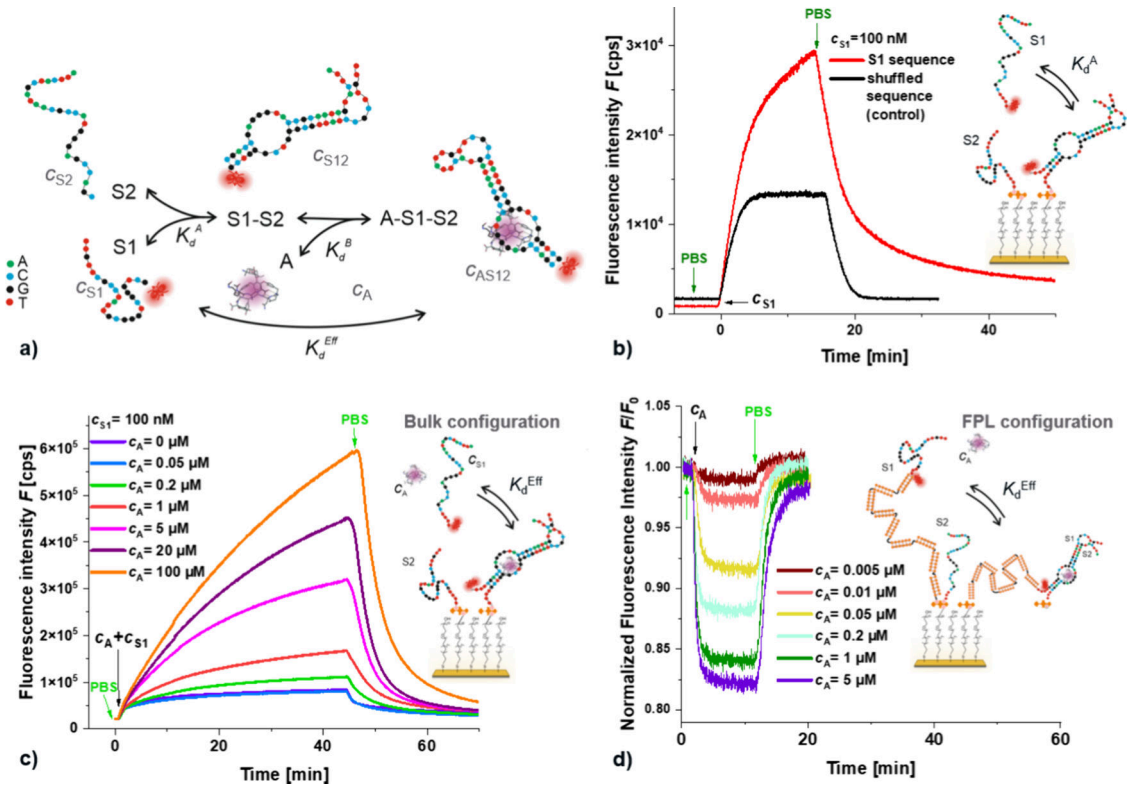

Figure 3. (a) Assumed model for the affinity interaction between split aptamer segments S1 and S2 and target analyte A. (b) Fluorescence intensity changes measured upon the affinity binding of S2 (attached to the sensor surface) to S1 (dissolved in the working buffer) at a concentration of c_{S1} = 100 nM. (c) Fluorescence intensity changes F measured for c_A = 50 nM–100 μM with S2 attached to the sensor surface to S1 present in the working buffer at a concentration of c_{S1} = 100 nM (bulk configuration). (d) Measured fluorescence intensity changes for both S1 and S2 attached to the sensor surface (FPL configuration) reacted with c_A = 5 nM–5 μM in the working buffer.

Split Aptamer Assay—Comparison with a Model

In order to analyze the response of the sensor, the dependence of the (equilibrium) sensor response ΔF on the concentration c_A was determined from experimental data (shown in Figure 3c,d) and is presented in Figure 4a (bulk configuration) and Figure 4b (FPL configuration). Interestingly, one can see that the bulk configuration shows a titration curve with an effective equilibrium dissociation constant of K_d^{Eff} = 5 μM, while the assay with the FPL configuration saturates at almost two orders of magnitude lower concentrations c_A corresponding to K_d^{Eff} = 70 nM. In order to explain such a difference in the assay readout relying on identical split aptamer pairs, we attempted to elucidate the interaction interplay between S1, S2, and A that allows for such tuning of the sensor detection range. We established a model describing the two-step reaction of S1 binding to S2 and subsequent affinity capture of analyte A with the S1–S2 complex (the respective differential equations can be found in the Supporting Information − eq S1–S4). This model is derived from SPR binding kinetics analysis and allows the determination of the fraction of c_{S1} and c_{S2} that hybridize (c_{S12}) to form an aptamer capable of binding the target analyte (c_{AS12}). The obtained results were compared with experimental data and are shown as lines in Figure 4a,b. In this model, we assume that the optical signal is defined by the fraction of S1 and S2 molecules in the unbound state (generating high fluorescence intensity F_{up}) and in the bound state (associated with low fluorescence intensity F_{down}) and that the system responds to the presence of the target analyte through stabilization of the S1–S2 bound state by capturing target analyte A.

In the bulk configuration, the S2 aptamer segment was attached to the surface, and the S1 aptamer segment was present in the bulk solution that was flowed over the surface. Therefore, we assumed that the concentration of free S1 molecules was not changing upon the affinity interaction with other assay constituents (c_{S1} = 100 nM). Then, the model yields the fraction of S2 strands that hybridized with S1 and captured target analyte A as follows:

$$\frac{c_{S12} + c_{AS12}}{c_{S2}} = \frac{1}{1 + \frac{1}{\frac{c_{S1}}{K_d^A}\left(1 + \frac{c_A}{K_d^B}\right)}} \quad (1)$$

For the FPL configuration with both S1 and S2 molecules confined on the surface, the total amount of S1 and S2 strands is constant, and the concentration of free strands S1 and S2 becomes depleted by mutual hybridization and affinity binding of A. Due to this fact, the respective differential equations lead to a more complicated form, and they were solved numerically. In the FPL configuration, the local concentration of c_{S1} and c_{S2} was determined from acquired surface densities by assuming that the reaction is restricted in a slice above the surface defined by the length and flexibility of FPL. Based on our previous study with the same design of the FPL, such a distance can be defined by a 3D random walk theory as the maximum end-to-end probability that yields 37 nm.[18] However, as the data in Figure 3c indicates, the stretching of FPL in the direction perpendicular to the surface

https://doi.org/10.1021/acssensors.5c03606
ACS Sens. 2026, 11, 1348−1357

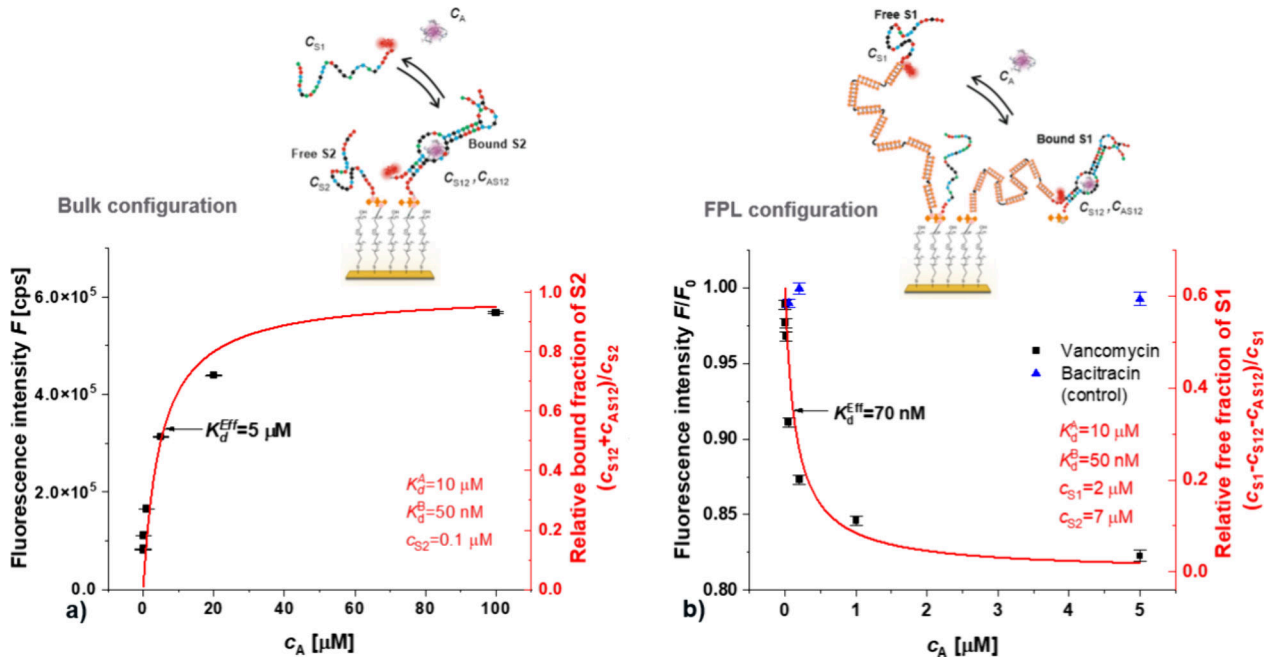

Figure 4. Titration curves for the sensor configuration determined for (a) bulk and (b) FPL configuration from the experimental data presented in Figure 3. The determined titration curves are compared to the model with parameters specified in the graphs. Error bars represent the baseline standard deviation of the equilibrium fluorescence signal.

is probably more restricted to $\Delta d \sim 15$ nm (as no increase in fluorescence intensity was observed when the emitter was immobilized on the surface). Therefore, the thickness of the slice was set to this value, and then surface density translates to local concentrations of $c_{S2} = 7$ μM and $c_{S1} = 2$ μM (in a volume defined by the slice of thickness Δd above the gold sensor surface, $c_{S1,2}$ is equal to surface density divided by Δd) and defines the ratio $c_{S2}/c_{S1} = 3.5$.

By comparing the experimental data in Figure 4a,b (squares) with the model (lines), we estimated the dissociation constants for the interaction between aptamer segments S1 and S2 (K_d^A) and the S1–S2 complex with target analyte A (K_d^B). The equilibrium constant K_d^A of S1 hybridization to S2 was identified as about 50 μM. Let us note that the DNA hybridization dissociation constant strongly depends on the number of complementary base pairs (bp), and for the values below 10, it was reported to decrease exponentially with the bp number.[23] The herein used hairpin structure exhibits 9 complementary bp segments, and for such length, a single-molecule interaction study reported a dissociation constant of 2–3 μM.[23,24] This about one order of magnitude difference can be explained by the effect of other parameters, such as the buffer composition and the DNA hairpin structure used here, which destabilizes duplexes and consequently increases the dissociation constant.[25] The determined equilibrium dissociation constant for the S1–S2 split aptamer interaction with target analyte A was fitted as $K_d^B = 10$ nM, and it can be compared with the equilibrium dissociation constant for its full-length version that was measured with a displacement fluorescence quenching assay.[9] This work estimated it as ~100 nM, and the difference with the herein obtained value K_d^B can be ascribed to the effect of splitting and the different assay format (the herein reported sandwich assay format compared to the competitive configuration used in ref 9).

The fact that the titration curve of the sensor relying on the interaction between S1, S2, and A strongly depends on the parameters of two interaction steps (marked as A and B in Figure 3a) is evident from the fact that the bulk and FPL configurations yield effective dissociation constants K_d^{Eff} differing by almost two orders of magnitude (even though the aptamer sequences S1 and S2 are the same). We attempt to explain these experimental observations by further simulations, where the dependence of the overall sensor response on the equilibrium constants K_d^A and K_d^B and on the concentrations c_{S1} and c_{S2} is investigated. These simulations are presented in Figure 5a,b, and for simplicity, we determined the fraction of S1 or S2 molecules (with the total concentration of c_{S1}) that are bound ($c_{S12} + c_{AS12}$) as a function of the target analyte concentration c_A (as the ratio $[c_{S12} + c_{AS12}]/c_{S1}$ directly relates to the measured fluorescence intensity changes).

First, the effect of increasing K_d^A (describing the S1–S2 interaction) is presented for the bulk configuration for fixed concentrations c_{S1} and c_{S2} in Figure 5a. It apparently shows a shift in the effective dissociation constant of the overall assay from $K_d^{Eff} = 9$ μM (for $K_d^A = 100$ μM) to $K_d^{Eff} < 1$ μM (for $K_d^A = 1$ μM). This effect occurs due to the increasing probability of S1 and S2 hybridization when decreasing K_d^A and thus the possibility of more frequent binding of target analyte A with $K_d^B < K_d^{Ef} < K_d^A$. Moreover, the obtained data show that when S1 and S2 affinity are allowed to interact strongly by decreasing K_d^A, a higher fraction of S1 and S2 is present in the hybridized state without the target analyte ($c_A = 0$), which leads to weaker modulation strength of the output signal when interacting with target analyte A. This effect is highlighted by marking the c_{S12} baseline in Figure 5a.

The other example of the dependency of the calibration curve on the concentration c_{S1} and c_{S2} is given in the data for the FPL configuration presented in Figure 5b for fixed K_d^A and K_d^B and constant ratio $c_{S2}/c_{S1} = 3.5$. The simulated titration curves show that the increasing concentration of c_{S1} from 0.3 to 300 μM leads to a shift in the effective dissociation constant from $K_d^{Eff} = 0.6$ μM to $K_d^{Eff} = 10$ nM. This trend shows almost matching K_d^{Eff} with K_d^B as S1 and S2 are more often available for binding target analyte A in their hybridized form S1–S2 when increasing their concentration

https://doi.org/10.1021/acssensors.5c03606
ACS Sens. 2026, 11, 1348−1357

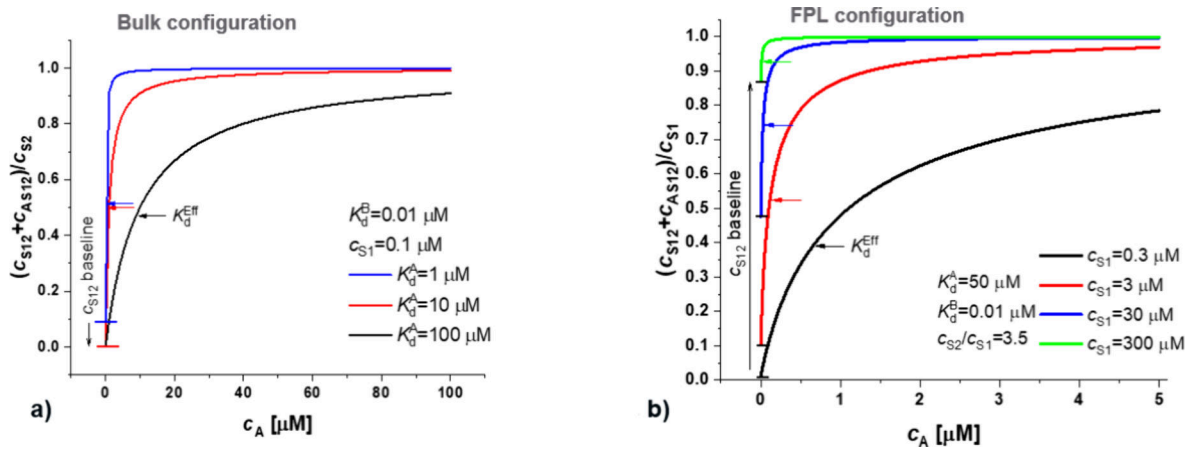

Figure 5. (a) Changes in the dependence of the equilibrium fraction of bound S2 split aptamer on the concentration of the target analyte c_A obtained by the model with varied K_d constant (affinity interaction between S1 and S2) and S1 present in the solution (bulk configuration). (b) Changes in the dependence of equilibrium fraction of bound S2 split aptamer on the concentration of target analyte c_A obtained by the model for concentrations c_{S1} and c_{S2} (ratio set to $c_{S2}/c_{S1} = 3.5$) when both S1 and S2 are present at the surface (FPL configuration).

above K_d^A. However, similar to the previous case, the modulation strength of the fraction split aptamer segments in the bound and unbound state is strongly decreased when c_{S1} and c_{S2} approach K_d^A. Then, the majority of split aptamer strands S1 and S2 become already hybridized even without target analyte A and lead to an increase of c_{S12} baseline (see Figure 5b). This effect would again impair the sensor performance as a weak sensor output signal modulation due to the affinity interaction with target analyte A would occur, which was experimentally observed in this work with PEF readout and FPL-based split aptamer confinement (Figure S4 in supporting information), as well as previous work with SPR readout and aptagel sensor format.[13]

Sensing Performance in the Working Buffer and Blood Plasma

Further, the characteristics of the reported sensor concept are evaluated when operated in working buffer and diluted blood plasma in terms of sensitivity to the target analyte and time resolution. First, calibration curves were established, and the LOD was obtained as a concentration c_A, where the sensor response change $\Delta F/F_0$ reaches the baseline noise described as standard deviation σ multiplied by a factor of 3. LOD was determined with the help of fitting the measured calibration curves with the Hill function (eq S5 in Supporting Information) and by solving $\Delta F/F_0(\mathrm{LOD}) = 3\sigma$. For the data measured in working buffer and presented in Figure 4b, an LOD of 4.1 nM was determined for $\sigma = 3.8 \times 10^{-3}$. Let us note that, as a negative control for the vancomycin calibration curve, the sensor output was measured for a structurally similar analyte, bacitracin (both are cyclic peptide antibiotics), as shown in Figure S5a. No significant change in the recorded signal F/F_0 confirms the specificity of the sensor toward the target vancomycin analyte A. Afterward, we investigated the robustness of the developed sensor when the detection of the target analyte was performed in human blood plasma diluted to 10% in the working buffer. Figure 6a shows the measured sensorgrams with the response F/F_0 for a series of samples spiked with the target analyte at increasing concentrations ranging from $c_A = 50$ nM to 20 μM. It shows three series of sample injecting and rinsing with 10% plasma (with $c_A = 0$) cycles after correction of the baseline F_0 that was extrapolated from the signal before and after each cycle (raw data are shown in Figure S6 with information on baseline normalization provided in Section 5, Supporting Information). The normalized equilibrium signals for each analyte concentration c_A and the generated calibration curve are presented in Figure 6b. This curve reflects the apparent concentration-dependent response of the sensor, and for the baseline standard deviation $\sigma = 2.98 \times 10^{-3}$, the LOD was calculated to be 19 nM.

Another important characteristic of the continuous monitoring sensor is the time resolution, which can be described by the time constant τ for the association and dissociation phases of the sensor response after injecting a sample with a changed analyte concentration c_A. Kinetic data in Figure 3b (working buffer) and Figure 6a (10% blood plasma) were fitted with the exponential function, and association/dissociation time values τ were obtained for each concentration ($c_A = 50$ nM−5 μM). The obtained values are compared in Figure 6c, and when standard deviations are taken into account, the association τ values of about 2 min for the response to lower analyte concentrations ($c_A = 0.05$−0.2 μM) in both 10% plasma and working buffer matrices. However, at higher concentrations ($c_A = 1$ and 5 μM), the association τ in diluted plasma is about two times higher than in buffer. Dissociation τ values were largely comparable between matrices across all concentrations, although a slight trend toward slower dissociation in plasma was observed at higher concentrations. The observed concentration-dependent sensor kinetics, where vancomycin binding is significantly slower in plasma at high analyte concentrations but similar to buffer at low concentrations, may be explained by competitive binding to high-affinity plasma proteins. At high total concentrations, the drug might be rapidly sequestered by abundant binders, primarily immunoglobulin A (IgA) and albumin, as documented in previous studies.[26,27] This instantaneous binding could create a "competitive sink" that reduces the concentration of free (unbound) vancomycin available to diffuse to the sensor surface. In addition, let us note that the observed association and dissociation constants are capturing diffusion-driven mass transfer of the molecules to and from the sensor surface.

Finally, an experiment was designed to monitor continuously changing amounts of the target analyte in 10% plasma by stepwise

https://doi.org/10.1021/acssensors.5c03606
ACS Sens. 2026, 11, 1348−1357

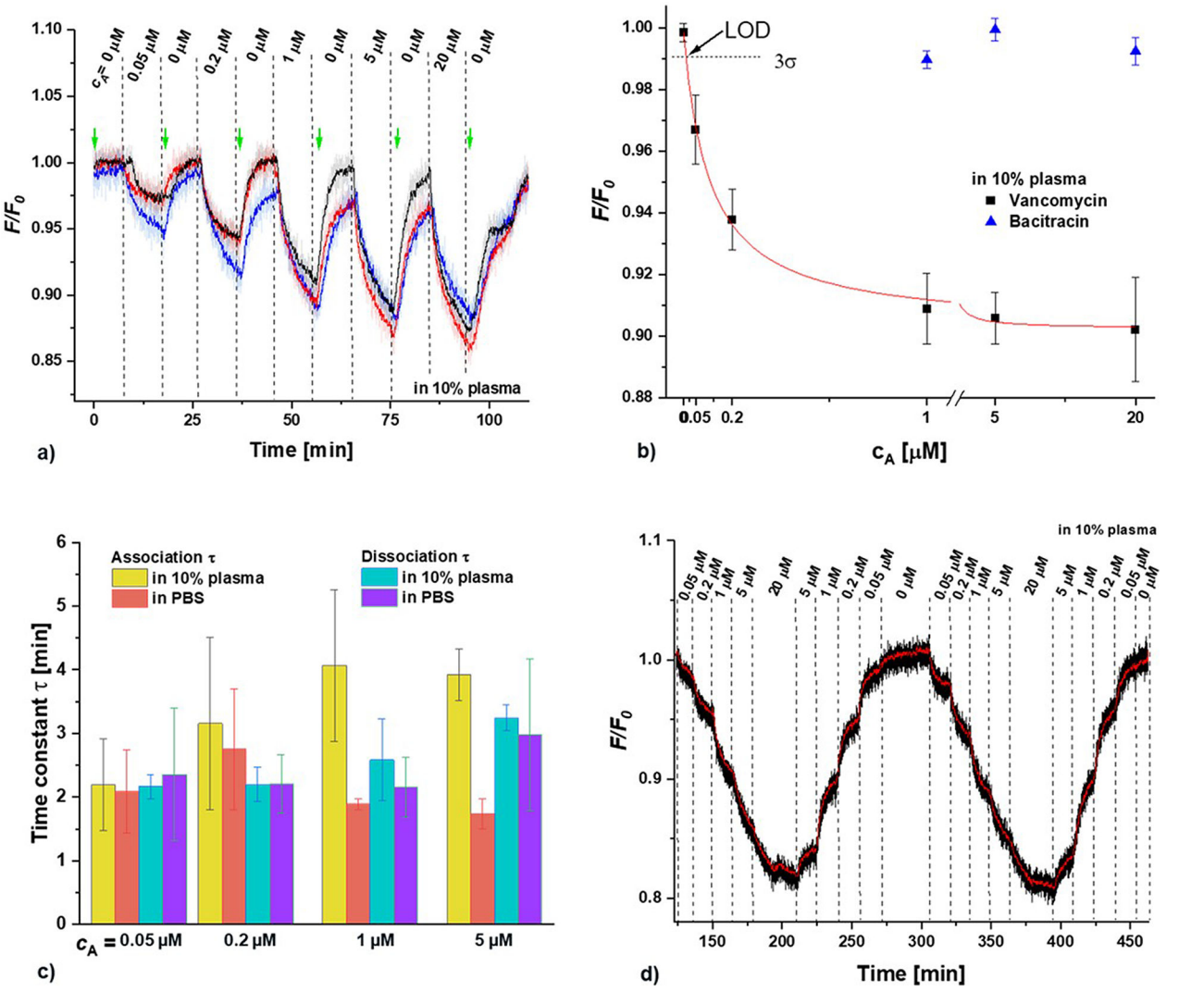

Figure 6. (a) Fluorescence response F obtained in three independent measurement cycles following an identical sequence of analyte injections in the FPL configuration with analyte concentrations of c_A = 50 nM−20 μM introduced in 10% human plasma. (b) Calibration curve for the target analyte vancomycin in 10% human plasma. Error bars represent the standard deviation of the equilibrium signal F/F_0. (c) Association and dissociation time constant τ as a function of analyte concentrations are shown in the working buffer and in 10% plasma. (d) Two cycles of continuous monitoring of the analyte in 10% plasma.

increasing the analyte concentration in the range of c_A = 50 nM−20 μM (without rinsing steps). The corresponding sensor signal F/F_0 is presented in Figure 6d (with raw data prior to the baseline correction F_0 provided in Figure S7). Notably, the sensor is capable of sustaining continuous monitoring for at least two full cycles (at least more than 7 h) of the given concentration series. The continuous, nonrinsed dataset is particularly important as it reflects the sensor response under uninterrupted analyte exposure, thereby revealing potential cumulative or matrix-dependent effects that may be masked when baseline recovery steps are included. This measurement mode better represents conditions encountered in real-time or continuous sensing applications.

In the present study, diluted plasma was intentionally employed to demonstrate and validate the core concept of the split-aptamer-based sensing strategy under biologically relevant conditions while maintaining experimental robustness. The extension of this approach to more complex biological matrices, such as whole blood or plasma, inevitably introduces additional considerations, and due to the higher refractive index, we could not employ the optical system used herein. In addition, one may expect more severe nonspecific adsorption of plasma proteins onto the biointerface that hinders analyte accessibility or signal transduction efficiency. In parallel, the presence of nucleases in biological fluids may affect the long-term stability of oligonucleotide aptamers, potentially impacting sensor longevity during prolonged operation. Moreover, variations in ionic strength and matrix composition may modulate aptamer folding and target-induced reassembly dynamics. Importantly, these effects are well recognized in biosensor development. Future efforts may therefore focus on refined surface passivation strategies[28,29] and chemical modifications to enhance aptamer robustness,[30] thereby further extending sensor performance in complex biological matrices.

CONCLUSIONS

This study demonstrates a novel split aptamer assay with a DNA-based FPL and a PEF readout for the continuous and sensitive monitoring of the low- molecular-weight antibiotic van-

https://doi.org/10.1021/acssensors.5c03606
ACS Sens. 2026, 11, 1348−1357

comycin. The biointerface architecture was designed to carry one split aptamer segment anchored via the FPL and the other split aptamer segment directly on the sensor surface at a controlled surface density and distance. Through interacting with the target analyte, the distance of the fluorophore tag (attached to the outer FPL end) to the metallic sensor surface was modulated and measured from the fluorescence intensity changes. The sensor concept proved the ability to monitor reversible binding kinetics of the vancomycin target analyte, which makes it suitable for real-time monitoring of concentration changes with a time resolution of several minutes and an LOD in the low nanomolar range. In addition, the biointerface design allows for the measurement in biologically relevant matrices such as diluted human plasma with a small sensitivity reduction due to matrix effects. Compared to previous split aptamer-based sensors with direct readout of reversible affinity interaction serving for continuous monitoring, the reported approach explores the tuning of sensor LOD and detection range by controlling the surface density of split aptamer parts. With the help of a model that describes the sequential binding of split aptamer segments and the target analyte capture, we elucidated the underlying mechanism and explained how the effective assay dissociation constant can be tuned (by several orders of magnitude), in parallel with experimentally observed changes in sensor output modulation strength. These findings can aid further development of a sensitive and tunable aptamer assay for various low-molecular-weight analytes important for TDM and personalized medicine applications. In particular, it may not only serve in the split aptamer configuration but may also relate to the full-length aptamer with conformation changes implemented in future continuous-monitoring biomedical devices.

■ ASSOCIATED CONTENT

Data Availability

The data that support the findings of this study are openly available in Zenodo (DOI: 10.5281/zenodo.17949560)

Supporting Information

The Supporting Information is available free of charge at https://pubs.acs.org/doi/10.1021/acssensors.5c03606.

Materials, chemicals, and experimental methods for sensor chip functionalization and SPR and SPFS measurements (PDF)

■ AUTHOR INFORMATION

Corresponding Author

Jakub Dostalek − *FZU-Institute of Physics, Czech Academy of Sciences, Na Slovance 2, Prague 182 21, Czech Republic; Danube Private University, Steiner Landstraße 124, Krems an der Donau 3500, Austria;* orcid.org/0000-0002-0431-2170; Email: dostalek@fzu.cz

Authors

Gizem Aktug − *FZU-Institute of Physics, Czech Academy of Sciences, Na Slovance 2, Prague 182 21, Czech Republic; Faculty of Mathematics and Physics, Charles University, Prague 121 16, Czech Republic;* orcid.org/0009-0005-2678-6851

Naoto Asai − *Danube Private University, Steiner Landstraße 124, Krems an der Donau 3500, Austria*

Anil Bozdogan − *Department of Laboratory Medicine, Division of Clinical Virology, Medical University of Vienna, Vienna 1090, Austria;* orcid.org/0000-0003-4790-6451

Catia Santa − *BioMed X Institute, Im Neuenheimer Feld 515, Heidelberg 69120, Germany*

Khulan Sergelen − *BioMed X Institute, Im Neuenheimer Feld 515, Heidelberg 69120, Germany*

Complete contact information is available at: https://pubs.acs.org/doi/10.1021/acssensors.5c03606

Funding

G.A. and J.D. are grateful for the support from the Czech Science Fund (GACR) project APLOMA (22-30456J). In addition, J.D. and G.A. were supported from the Operational Programme Johannes Amos Comenius financed by European Structural and Investment Funds and the Czech Ministry of Education, Youth and Sports (Project No. SENDISO -CZ.02.01.01/00/22_008/0004596). G.A. was supported by Charles University through SVV-2023-260716. J.D. and N.A. were supported by Gesellschaft für Forschungsförderung Niederösterreich m.b.H. project FTI24-G-027.

Notes

The authors declare no competing financial interest.

■ REFERENCES

(1) Yan, J.; van Smeden, L.; Merkx, M.; Zijlstra, P.; Prins, M. W. J. Continuous Small-Molecule Monitoring with a Digital Single-Particle Switch. *ACS Sens.* **2020**, *5* (4), 1168–1176.

(2) Zargartalebi, H.; Mirzaie, S.; GhavamiNejad, A.; Ahmed, S. U.; Esmaeili, F.; Geraili, A.; Flynn, C. D.; Chang, D.; Das, J.; Abdrabou, A.; et al. Active-reset protein sensors enable continuous in vivo monitoring of inflammation. *Science* **2024**, *386* (6726), 1146–1153.

(3) Thompson, I. A. P.; Saunders, J.; Zheng, L.; Hariri, A. A.; Maganzini, N.; Cartwright, A. P.; Pan, J.; Yee, S.; Dory, C.; Eisenstein, M.; et al. An antibody-based molecular switch for continuous small-molecule biosensing. *Sci. Adv.* **2023**, *9* (38), No. eadh4978.

(4) Lamberti, V.; Dolci, M.; Zijlstra, P. Continuous Monitoring Biosensing Mediated by Single-Molecule Plasmon-Enhanced Fluorescence in Complex Matrices. *ACS Nano* **2024**, *18* (7), 5805–5813.

(5) Bian, S.; Zhu, B.; Rong, G.; Sawan, M. Towards wearable and implantable continuous drug monitoring: A review. *J. Pharm. Anal.* **2021**, *11* (1), 1–14.

(6) McKeating, K. S.; Aubé, A.; Masson, J. -F. Biosensors and nanobiosensors for therapeutic drug and response monitoring. *Analyst* **2016**, *141* (2), 429–449.

(7) Goncales, V.; Chamazketi, A. A.; Harrison, M.; Leung, K.; Gerson, J.; Batchelor, R. H.; Farnkopf, A.; Hodges, A.; Plaxco, K. B-301 In-vivo Continuous Therapeutic Drug Monitoring With Electrochemical Aptamer-based Sensors. *Clin. Chem.* **2023**, *69* (Supplement_1), No. hvad097-621.

(8) Lin, S.; Cheng, X.; Zhu, J.; Wang, B.; Jelinek, D.; Zhao, Y.; Wu, T.-Y.; Horrillo, A.; Tan, J.; Yeung, J.; et al. Wearable microneedle-based electrochemical aptamer biosensing for precision dosing of drugs with narrow therapeutic windows. *Sci. Adv.* **2022**, *8* (38), No. eabq4539.

(9) Dauphin-Ducharme, P.; Yang, K.; Arroyo-Currás, N.; Ploense, K. L.; Zhang, Y.; Gerson, J.; Kurnik, M.; Kippin, T. E.; Stojanovic, M. N.; Plaxco, K. W. Electrochemical Aptamer-Based Sensors for Improved Therapeutic Drug Monitoring and High-Precision, Feedback-Controlled Drug Delivery. *ACS Sens.* **2019**, *4* (10), 2832–2837.

(10) Arroyo-Currás, N.; Somerson, J.; Vieira, P. A.; Ploense, K. L.; Kippin, T. E.; Plaxco, K. W. Real-time measurement of small molecules directly in awake, ambulatory animals. *Proc. Natl. Acad. Sci. U. S. A.* **2017**, *114* (4), 645–650.
(11) Shaver, A.; Mahlum, J. D.; Scida, K.; Johnston, M. L.; Aller Pellitero, M.; Wu, Y.; Carr, G. V.; Arroyo-Currás, N. Optimization of Vancomycin Aptamer Sequence Length Increases the Sensitivity of Electrochemical, Aptamer-Based Sensors In Vivo. *ACS Sens.* **2022**, *7* (12), 3895–3905.
(12) Santa, C.; Park, S.; Gejt, A.; Clark, H. A.; Hengerer, B.; Sergelen, K. Real-time monitoring of vancomycin using a split-aptamer surface plasmon resonance biosensor. *Analyst* **2025**, *150* (1), 131–141.
(13) Park, S.; Gerber, A.; Santa, C.; Aktug, G.; Hengerer, B.; Clark, H. A.; Jonas, U.; Dostalek, J.; Sergelen, K. Molecularly Responsive Aptamer-Functionalized Hydrogel for Continuous Plasmonic Biomonitoring. *J. Am. Chem. Soc.* **2025**, *147* (13), 11485–11500.
(14) Patel, S.; Preuss, C. V.; Bernice, F. Vancomycin. In *StatPearls*; StatPearls Publishing LLC.: Treasure Island (FL), 2025.
(15) Vazquez-Guillamet, C.; Kollef, M. H. Treatment of Gram-positive infections in critically ill patients. *BMC Infect. Dis.* **2014**, *14*, No. 92.
(16) Pyle-Eilola, A. L. Chapter 8 - Guidelines for monitoring vancomycin, aminoglycosides, and other antibiotics. In *Therapeutic Drug Monitoring*, 2nd edition; Dasgupta, A., Ed.; Academic Press, 2024; pp 197–215
(17) Debiais, M.; Lelievre, A.; Smietana, M.; Müller, S. Splitting aptamers and nucleic acid enzymes for the development of advanced biosensors. *Nucleic Acids Res.* **2020**, *48* (7), 3400–3422.
(18) Asai, N.; Schmidt, K.; Aktuğ, G.; Fossati, S.; Sladek, J.; Lynn, N. S.; Jr. Dostalek, J. Tethered Catalytic Hairpin Assembly with Plasmon-Enhanced Fluorescence Readout for Single Molecule Detection. *Small Methods* **2025**, *9*, No. 2500037.
(19) Stothard, P. *The Sequence Manipulation Suite: JavaScript programs for analyzing and formatting protein and DNA sequences*. 2000 Available from: https://www.bioinformatics.org/sms2/shuffle_dna.html (accessed August 13, 2025).
(20) Mor, D. C.; Aktug, G.; Schmidt, K.; Asokan, P.; Asai, N.; Huang, C.-J.; Dostalek, J. Plasmon-enhanced fluorescence (bio)sensors and other bioanalytical technologies. *TrAC Trends Anal. Chem.* **2025**, *183*, No. 118060.
(21) Sergelen, K.; Fossati, S.; Turupcu, A.; Oostenbrink, C.; Liedberg, B.; Knoll, W.; Dostálek, J. Plasmon Field-Enhanced Fluorescence Energy Transfer for Hairpin Aptamer Assay Readout. *ACS Sens.* **2017**, *2* (7), 916–923.
(22) Berlier, J. E.; Rothe, A.; Buller, G.; Bradford, J.; Gray, D. R.; Filanoski, B. J.; Telford, W. G.; Yue, S.; Liu, J.; Cheung, C.-Y.; et al. Quantitative Comparison of Long-wavelength Alexa Fluor Dyes to Cy Dyes: Fluorescence of the Dyes and Their Bioconjugates. *J. Histochem. Cytochem.* **2003**, *51* (12), 1699–1712.
(23) Dupuis, N. F.; Holmstrom, E. D.; Nesbitt, D. J. Single-molecule kinetics reveal cation-promoted DNA duplex formation through ordering of single-stranded helices. *Biophys. J.* **2013**, *105* (3), 756–766.
(24) Jungmann, R.; Steinhauer, C.; Scheible, M.; Kuzyk, A.; Tinnefeld, P.; Simmel, F. C. Single-Molecule Kinetics and Super-Resolution Microscopy by Fluorescence Imaging of Transient Binding on DNA Origami. *Nano Lett.* **2010**, *10* (11), 4756–4761.
(25) Schreck, J. S.; Ouldridge, T. E.; Romano, F.; Šulc, P.; Shaw, L. P.; Louis, A. A.; Doye, J. P. DNA hairpins destabilize duplexes primarily by promoting melting rather than by inhibiting hybridization. *Nucleic Acids Res.* **2015**, *43* (13), 6181–6190.
(26) Sun, H.; Maderazo, E. G.; Krusell, A. R. Serum protein-binding characteristics of vancomycin. *Antimicrob. Agents Chemother.* **1993**, *37* (5), 1132–1136.
(27) Butterfield, J. M.; Patel, N.; Pai, M. P.; Rosano, T. G.; Drusano, G. L.; Lodise, T. P. Refining Vancomycin Protein Binding Estimates: Identification of Clinical Factors That Influence Protein Binding. *Antimicrob. Agents Chemother.* **2011**, *55* (9), 4277–4282.
(28) Vaisocherová, H.; Yang, W.; Zhang, Z.; Cao, Z.; Cheng, G.; Piliarik, M.; Homola, J.; Jiang, S. Ultralow Fouling and Functionalizable Surface Chemistry Based on a Zwitterionic Polymer Enabling Sensitive and Specific Protein Detection in Undiluted Blood Plasma. *Anal. Chem.* **2008**, *80* (20), 7894–7901.
(29) Chou, Y. N.; Sun, F.; Hung, H. C.; Jain, P.; Sinclair, A.; Zhang, P.; Bai, T.; Chang, Y.; Wen, T. C.; Yu, Q.; et al. Ultra-low fouling and high antibody loading zwitterionic hydrogel coatings for sensing and detection in complex media. *Acta Biomater.* **2016**, *40*, 31–37.
(30) Kratschmer, C.; Levy, M. Effect of Chemical Modifications on Aptamer Stability in Serum. *Nucleic Acid Ther.* **2017**, *27* (6), 335–344.

https://doi.org/10.1021/acssensors.5c03606
ACS Sens. 2026, 11, 1348–1357